Journal of
Mechanics of Materials and Structures

A NUMERICAL INVESTIGATION OF THE EFFECT OF BOUNDARY CONDITIONS AND REPRESENTATIVE VOLUME ELEMENT SIZE FOR POROUS TITANIUM

Hui Shen and L. Catherine Brinson

Volume 1, Nº 7 *September 2006*

mathematical sciences publishers

JOURNAL OF MECHANICS OF MATERIALS AND STRUCTURES
Vol. 1, No. 7, 2006
dx.doi.org/10.2140/jomms.2006.1.1179

msp

A NUMERICAL INVESTIGATION OF THE EFFECT OF BOUNDARY CONDITIONS AND REPRESENTATIVE VOLUME ELEMENT SIZE FOR POROUS TITANIUM

HUI SHEN AND L. CATHERINE BRINSON

To facilitate the design and application of porous titanium and titanium foam, numerical simulation of their mechanical behavior is essential. The concept of a representative volume element (RVE) is essential to obtain accurate estimates of the properties. Because of the high contrast between the properties of the two phases (pore vs. matrix), it is impractical to obtain a single RVE independent of boundary conditions to provide accurate predictions. We suggest that a set of small domain RVEs can be used instead, as long as the average of the small domains provides a convergent result. Two mixed boundary conditions simulating uniaxial proportional loading were designed and implemented on several 2D and 3D finite element models at different length scales, that is, containing different numbers of pores. The two boundary conditions provide opposite biased responses. Convergence of both the macroscopic and the microscopic elastoplastic responses associated with the boundary conditions is demonstrated here. By this approach, RVEs that are prohibitively large according to Hill's definition are divided into reasonably small ones associated with special boundary conditions, and the error of predictions associated with model size can be estimated.

1. Introduction

Pure titanium and titanium-based alloys exhibit very useful mechanical and biological properties, which make titanium-based foams potential materials for load-bearing sandwich cores and orthopedic implants [Banhart 2001; Spoerke et al. 2005; Wen et al. 2002a; Wen et al. 2002b]. In particular, we observe that as a potential implant material, it is comparable to bone stiffness in that its stiffness as a porous material drops with the square of relative density, and the open porosity allows complete bone ingrowth [Gibson and Ashby 1997; Spoerke et al. 2005]. These properties make porous titanium a promising material to solve the inherent problems of monolithic metallic implants, such as the "stress shielding" effect [Chang et al. 1996; Dunand 2004; Li et al. 2004; Spoerke et al. 2005; Wen et al. 2002a; Wen et al. 2002b]. However, the porous microstructure of the foam leads to the concentration of stress and strain near pores under load-bearing conditions, which results in reduced strength and ductility. Finite element (FE) simulation on a microstructural level is therefore needed to understand and predict the macroscopic and microscopic responses, to better target and optimize the application of these porous materials.

The titanium foam considered here was processed by a solid-state foaming technique in which individual high-pressure argon pores expand at elevated temperature and coalesce to form large pores

The authors acknowledge the financial support of the National Science Foundation through grant number DMR-0108342 and thank Professor Dunand's group for providing titanium foam and images.
Keywords: representative volume element, titanium foam, microstructure, finite element, boundary condition.

[Dunand 2004; Murray and Dunand 2003]. When porosity is less than 25%, pores are mostly rounded, generally equiaxial, and unmerged (see Figure 1 (top)). As higher porosity, small pores coexist with large pores which have a complex, tortuous shape, as shown in Figure 1 (bottom) [Murray and Dunand 2003]. The microstructures are locally heterogeneous, although sufficiently large experimental samples behave homogeneously. For such a heterogeneous material, it is fundamental to determine whether a FE model that simulates a fragment of the heterogeneous microstructure is large enough to be a representative volume element (RVE) to describe the responses of the titanium foam. The determination of the minimum size of an RVE relies on basic definitions, which have been developed for the study of heterogeneous materials. One definition, proposed by [Hill 1963], states that an RVE is "a sample that (a) is structurally entirely typical of the whole mixture on average, and (b) contains a sufficient number of inclusions for the apparent overall moduli to be effectively independent of the surface values of traction and displacement, so long as these values are macroscopically uniform." Point (a) requires the RVE to include statistically all possible microstructural configurations, and (b) demands that the effective properties obtained from the RVE be independent of the uniform displacement and traction boundary conditions (BCs). Regarding (b), Huet [1990] analytically proved that the effective elastic modulus obtained from an RVE is bounded by the average apparent responses of finite size domains under uniform displacement boundary condition (UDBC) and uniform traction boundary condition (UTBC). This conclusion was extended to a nonlinear elastic heterogeneous material by [Hazanov 1999] and to elastoplastic materials under proportional loading by [Jiang et al. 2001b]. Subsequently, many researchers have shown homogenization convergence such that as the domain size increases to the minimum RVE, the two bounds converge to the effective property [Hollister and Kikuchi 1992; Huet 1990; Jiang et al. 2001a; Ostoja-Starzewski 1998; Pecullan et al. 1999; Terada et al. 2000]. However, the convergence of the two bounds was found to be extremely slow for heterogeneous materials with soft inclusions in a hard matrix, and the higher the contrast between the moduli of matrix and inclusions, the slower the convergence [Bouyge et al. 2002; Jiang et al. 2001a; Ostoja-Starzewski 1998; Pecullan et al. 1999]. Given that zero-modulus pores provide extreme moduli contrast to the titanium matrix for the titanium foam, the minimum RVE according to Hill's definition becomes too large for FE analyses, especially for three dimensional (3D) FE analyses, due to the limitation of computational power.

A more pragmatic definition of RVE was introduced by [Drugan and Willis 1996], which defines it as "the smallest material volume element of the composite for which the usual spatially constant 'overall modulus' macroscopic constitutive representation is a sufficient accurate model to represent mean constitutive response." Based on this RVE concept, Drugan and Willis [1996] analytically proved that it is possible to obtain relatively accurate estimations of elastic constants with small RVEs for a microstructure with nonoverlapping spherical inclusions. In particular, the effective moduli obtained by a finite size domain over a length of only two sphere diameters can be close to those obtained by a domain of infinite length, within a few percent of error, even in cases of void inclusions. This conclusion contradicts the results obtained according to Hill's definition. The BC applied on the RVE is the key factor responsible for the difference. Although the RVE should be independent of BCs according to Hill's definition, the right BC is needed for the RVE defined by [Drugan and Willis 1996]. As pointed out by [Jiang et al. 2001a], the derivation of [Drugan and Willis 1996] for the minimum RVE implied that the RVE should be associated with periodic BC and that the microstructure is actually periodic. They verified the RVE theory of [Drugan and Willis 1996] for unidirectional fiber-matrix composites with the

modulus contrast of inclusion to matrix in a range of 0.001 to 1000. Gusev [1997] numerically verified that the average of elastic constants of many small RVEs is close to the result for large RVEs for 3D microstructures with randomly distributed nonoverlapping spherical inclusions under periodic BC. Their results also indicate that smaller analyzed windows lead to more scattered results.

Following the concept of the RVE defined by [Drugan and Willis 1996] but accounting for the fluctuations of the apparent properties predicted by finite size domains, Kanit et al. [2003] recently proposed a more quantitative definition. Based on their definition, the concept of one single minimum RVE should be abandoned and a sufficient number of small domain RVEs should be used to obtain the average linear properties. While UTBC and UDBC on small domains result in large, oppositely biased errors for the effective property, a periodic BC gives a smaller error for the same window size. However, it should be noted that periodic BC requires the continuity of the inclusions on opposite boundaries to ensure the periodicity of the microstructure. Because such unnatural periodicity is seldom observed in real heterogeneous materials, periodic BCs are not appropriate for FE models developed by cutting out fragments of actual microstructures or by using simulated microstructures based on actual microstructures.

Alternative BCs might be considered which maintain the philosophy of the RVE concept of Kanit et al. [2003], that is, which emphasize the average of the responses of small domains. Hazanov and Huet [1994] proved analytically that the elasticity tensor predicted by a model smaller than Hill's RVE definition submitted to mixed BCs falls between the predictions associated with UTBC and UDBC. They concluded that relatively accurate results can be obtained by using small domains under mixed BCs. Jiang et al. [2001a] numerically verified this conclusion on unidirectional fiber-matrix composites. However, the kind of mixed BCs to associate with RVEs to obtain accurate estimates for porous microstructure is still an open question. Because of the extreme contrast in properties between inclusion and matrix, no satisfactory solution (achievable with reasonable computer power) yet exists for practical RVEs for porous microstructure.

The objective of this paper is to find reliable and practical RVEs for porous titanium using the homogenization convergence concept and obtaining statistical averages by solving the boundary value problems. As discussed above, solutions of finite size domains under mixed BCs approach effective properties much faster than UDBC and UTBC. However, since results from finite size domains under a single mixed BC approach the effective properties from one side, it is difficult to determine the point where the finite size domains are large enough. In addition, such a one-side bias can be eliminated only by increasing the size of analyzed domains. Therefore, we designed two mixed BCs simulating a uniaxial loading condition providing opposite bias and imposed them on the porous models. This enabled us to determine the convergence of RVEs and obtain relatively accurate results with small RVEs by averaging the results associated with the two BCs. By this approach, we trade-off the large RVEs with two mixed BCs and more small domains. In other words, the prohibitively large RVE of Hill's definition were divided into reasonable small ones associated with special BCs. While previous definitions of RVE focused only on macroscopic linear properties, our current study also aims to verify the convergence of both the macroscopic and the microscopic elastoplastic responses. The results of this paper elucidate a method for numerical prediction of the global and local response with small size models for porous materials.

It should be noted that a porosity of 40–50% is generally considered to be an ideal range for orthopedic applications of porous titanium. This porosity provides reduced stiffness for reduced stress-shielding as well as sites for bone ingrowth, while simultaneously maintaining mechanical durability. However, the

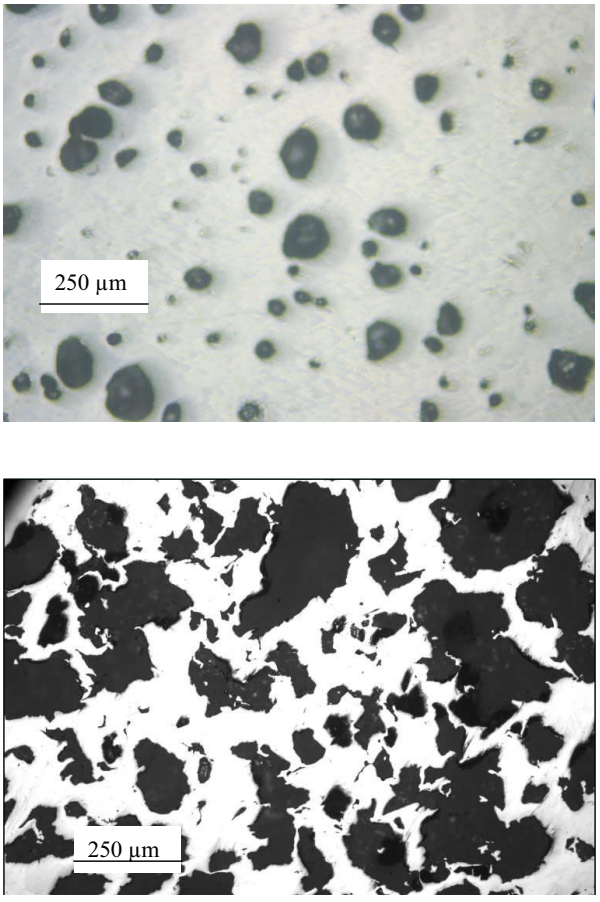

Figure 1. Optical micrograph of metallographic cross-section for titanium foam with 14.7% porosity (top) and 50% porosity (bottom).

microstructure at such high porosity is extremely complex (see, for example, Figure 1 (bottom)). Since we focus on exploring methodology in this current study, we present results for low porosity titanium foam and discuss implications for a 3D model with a higher porosity of 48%. The RVE for higher porosity titanium foams will be considered in our future work.

In next sections, 2D and 3D FE models with different sizes are created based on the simulated microstructure of the experimental material using the methodology presented in our previous work [Shen et al. 2006]. BCs for the FE simulations are described. Then the uniaxial stress-strain response is simulated based on the FE models associated with the two mixed BCs. Both macroscopic and microscopic responses are demonstrated for the convergence study.

2. Finite element modeling

2.1. ***Simulated microstructure.*** We generated a simulated version of the microstructure of the titanium foam at 14.7% porosity using the methodology presented in our previous work [Shen et al. 2006]. 3D pore size and location distribution information was first derived from 2D sections of a sample at 14.7%

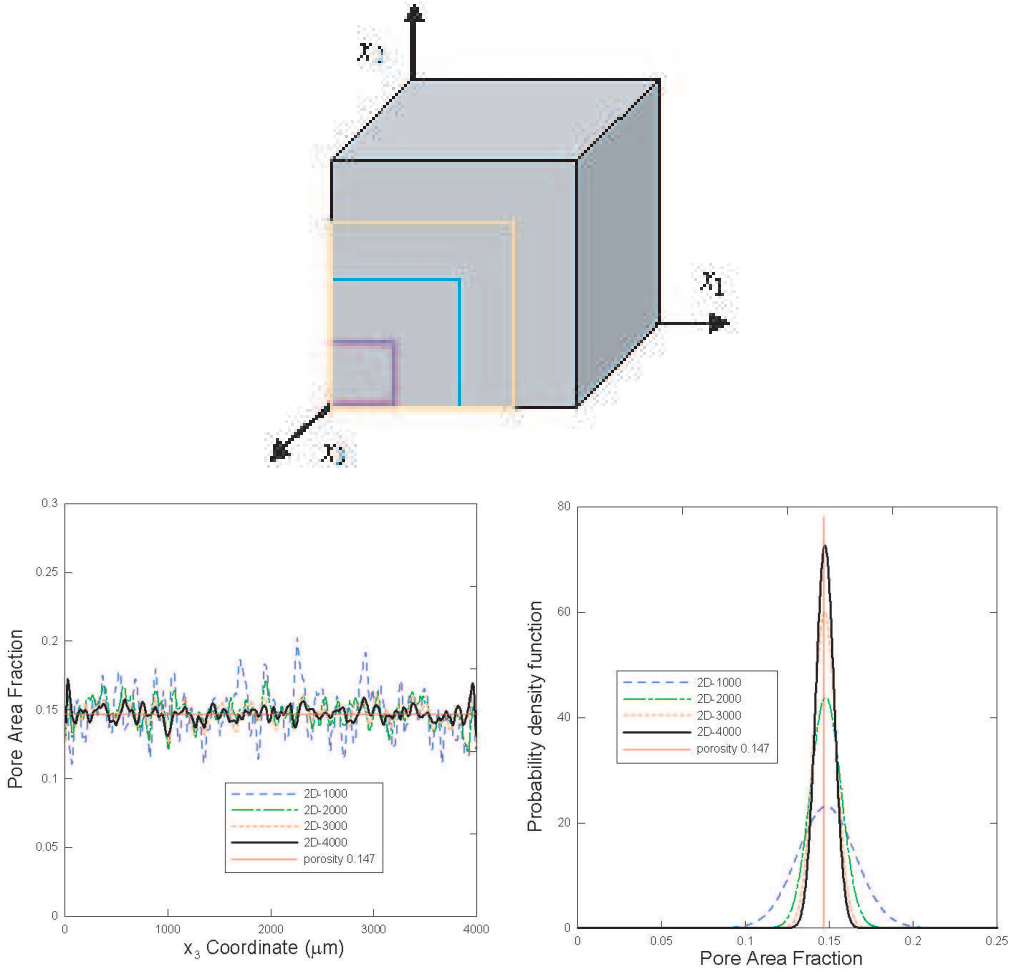

Figure 2. The cubic domain of the 3D-MP-70271 model with side length of 4000 μm and a series of window sizes of 1000 μm, 2000 μm, 3000 μm, and 4000 μm (top). Pore area fraction as a function of the x_3 position for the series of windows (bottom left). Distributions of pore area fraction of each window series (bottom right).

porosity as shown in Figure 1 (top). The location distribution of pores is random. The pore size distribution follows the Weibull distribution [Tobias and Trindade 1995] in which the density function is denoted by

$$f(x) = \frac{m}{x}\left(\frac{x}{c}\right)^m e^{-(x/c)^m},$$

where the parameters, m and c, are shape and scale parameters. We obtained $m = 2.47$ and $c = 64.68$ for the pore sections observed in 2D sectioning planes, observing an average diameter of 63.3 μm. We derived $m = 2.29$ and $c = 60.52$ by stereology study, resulting in 3D average pore diameter of 53.6 μm [Shen et al. 2006]. Based on these data, a 3D simulated microstructure which retains the essential geometry features of the random microstructure was developed. The microstructure of the foam at higher

porosity was determined by a geometric simulation of pore growth and movement during the foaming process.

In the simulated 3D multipore microstructure (3D-MP-70271) at porosity 14.7%, 70,271 spherical pores were randomly located in a $(4000\,\mu\text{m})^3$ cube. No pore impingement was permitted. To simulate the serial sectioning process, a reliable technique for constructing microstructures [Li et al. 1998], sections parallel to the x_1x_2 plane passed through the 3D-MP-70271 model were cut every $10\,\mu$m along x_3 axis.

The distribution of pore area fractions in window sizes of $1000\,\mu$m, $2000\,\mu$m, $3000\,\mu$m, and $4000\,\mu$m is shown in Figure 2. We see that as the size of the window increases, the range and variation of the area fraction decreases and the area fractions converge to the overall porosity of the microstructure.

The simulated microstructure is comprised of two distinct phases: pores and titanium matrix. To avoid computational difficulties, it was assumed that pores are linear elastic with a very low modulus of 10^{-7} GPa and Poisson's ratio of 0.3. The titanium matrix having elastic modulus of 110 GPa, Poisson's ratio of 0.33, and yield strength of 275 MPa is representative of CP Ti-40 [ASM 2002]. The matrix yield surface follows the Von Mises yield criterion with isotropic hardening. All material properties and simulations are for room temperature.

2.2. ***2D and 3D finite element models.*** 2D and 3D finite element models were created by cutting out the fragments of the simulated microstructure. To study the convergence of responses of various size windows, four groups of 2D sections of side length from $1000\,\mu$m to $4000\,\mu$m having an area fraction matching the overall porosity of 14.7% were generated based on the simulated microstructure to construct 2D models. The four groups of 2D finite element models with side lengths of $1000\,\mu$m, $2000\,\mu$m, $3000\,\mu$m, and $4000\,\mu$m have ratios of model length to the average pore size (L/d) of 15.8, 31.6, 47.4, and 63.2, respectively. Each model group contains eight models and is labeled with the size, that is, side length. For example, 2D-1000 refers to the model group with side length of $1000\,\mu$m. Examples of these 2D model groups are shown in Figure 3. We see that some pores having a centroid near an edge are truncated. On average, there are 59 pores and 10,930 elements in the 2D-1000 model; 235 pores and 39,010 elements in the 2D-2000 model; 542 pores and 88,385 elements in the 2D-3000 model; 943 pores and 159,768 elements in the 2D-4000 model.

Two 3D model groups with side lengths of $170\,\mu$m and $340\,\mu$m having porosity of 14.7% were selected from different locations of the 3D-MP-70271 microstructure. Each group contains four 3D models. The ratios of model size to the average pore size (L/d) are 3.17 and 6.34, respectively. Models are labeled with the two sizes as 3D-170 and 3D-340. Examples of the 3D-170 and 3D-340 models are shown in Figure 4. Again, some pores having a centroid near a face are truncated. On average, the 3D-170 model contain 12 pores and 15,439 elements; the 3D-340 model 64 pores and 125,536 elements.

One 3D model with higher porosity of 48% in a $340\,\mu$m cube was created by cutting a block of a high porosity microstructure. As shown in Figure 5, pores are connected to form large pores which have a complex, tortuous shape. The model contains 130,552 elements.

All 2D models were meshed with eight-node biquadratic plane strain elements and all 3D models were meshed with ten-node modified tetrahedral elements with hourglass control to prevent volumetric lock during plastic deformation [ABAQUS 2004]. All finite element analyses were performed using ABAQUS software. Mesh convergence was verified based on overall and local stress values. The overall

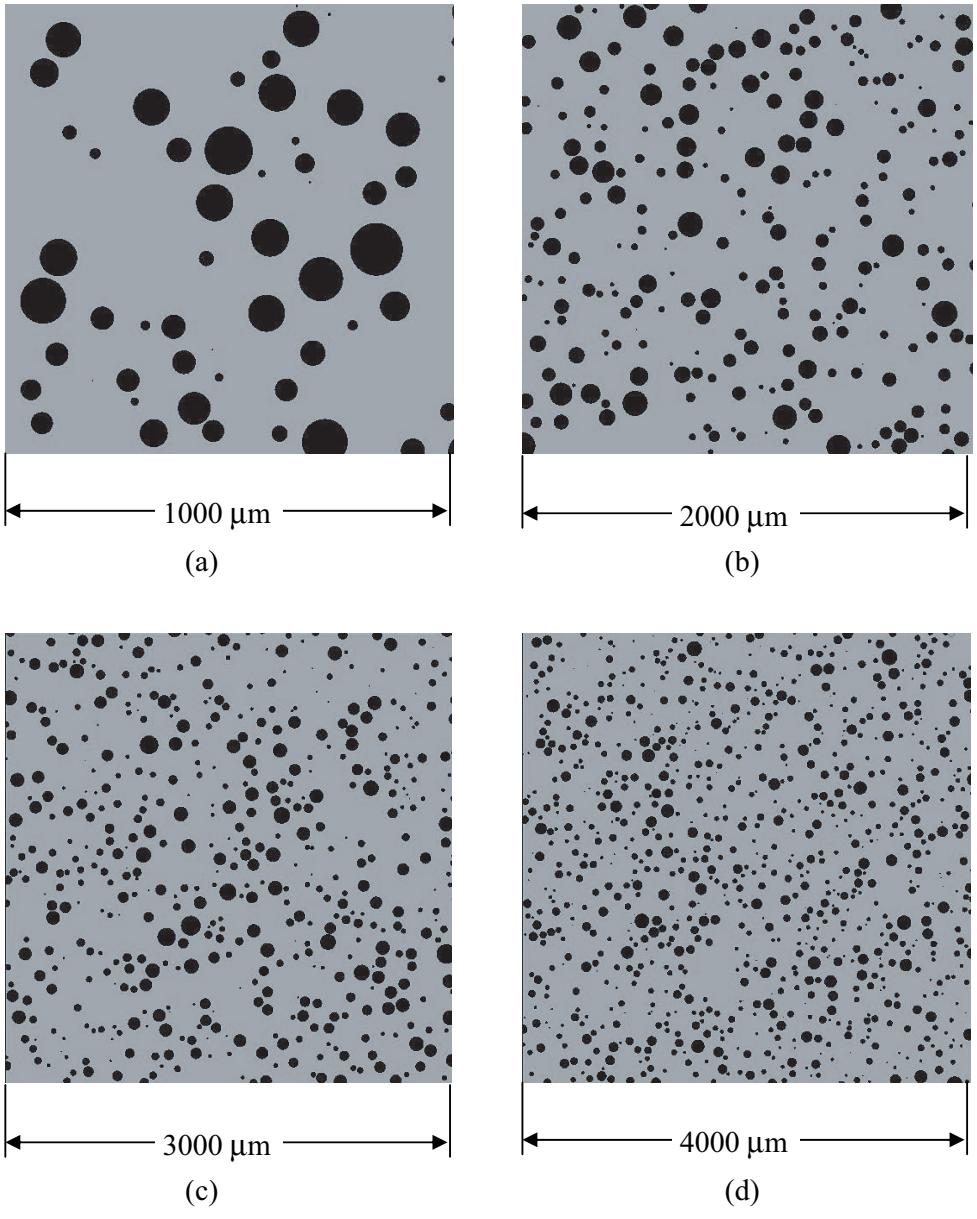

Figure 3. Geometry of the (a) 2D-1000, (b) 2D-2000, (c) 2D-3000, and (d) 2D-4000 models.

strain and stress are calculated by using volume averages

$$\bar{\varepsilon}_{ij} = \frac{1}{V}\int_V \varepsilon_{ij} dV = \frac{1}{\sum_{m=1}^{N} V^{(m)}} \sum_{m=1}^{N} \varepsilon_{ij}^{(m)} V^{(m)},$$

$$\bar{\sigma}_{ij} = \frac{1}{V}\int_V \sigma_{ij} dV = \frac{1}{\sum_{m=1}^{N} V^{(m)}} \sum_{m=1}^{N} \sigma_{ij}^{(m)} V^{(m)}.$$

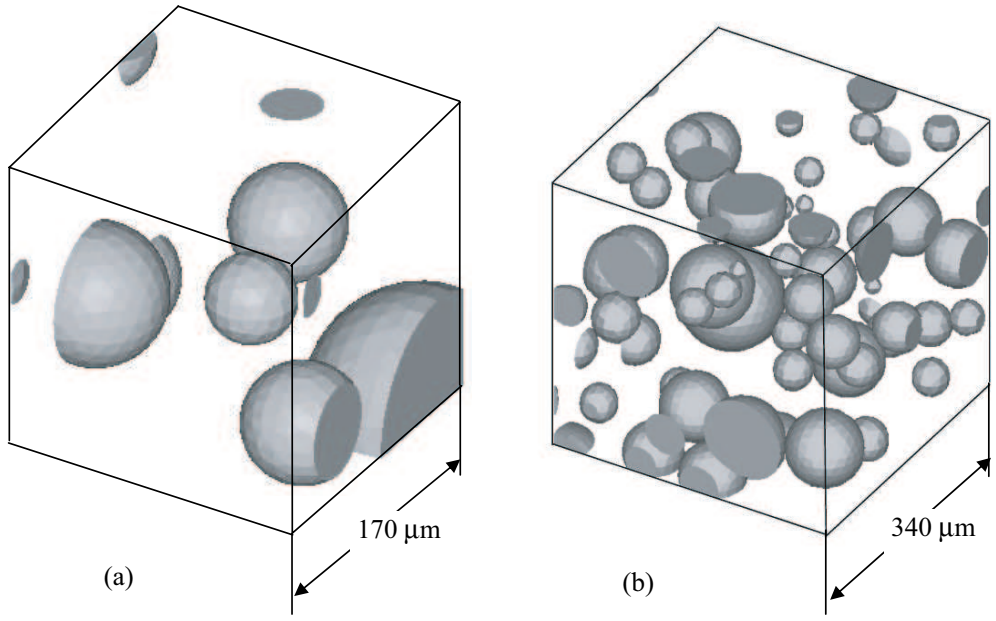

Figure 4. Geometry of the (a) 3D-170 and (b) 3D-340 models.

The standard deviation of the microscopic stress distribution is weighted by the volume of the element as follows:

$$SD = \sqrt{\frac{\sum_{m=1}^{N} V^{(m)}(\sigma_{ij}^{(m)} - \overline{\sigma}_{ij})^2}{\sum_{m=1}^{N} V^{(m)}}},$$

where $V^{(m)}$ is the volume of element m, N is the total number of elements, and σ_{ij} is the Cauchy stress tensor. The total strain tensor is decomposed into elastic and plastic components. Note that the stress and strain tensors σ_{ij} and ε_{ij} are obtained at the centroid of each element.

2.3. ***Boundary conditions.*** The experimental procedure to obtain macroscopic stress-strain response for porous materials is typically a uniaxial compression test, which has been performed for porous titanium in [Davis et al. 2001] and [Shen et al. 2006]. Our numerical study focuses on the responses of the titanium foam under uniaxial proportional compressive loading. As discussed in Section 1, one can obtain accurate estimates of material properties with relatively small RVEs under mixed BCs [Hazanov and Huet 1994]. Two types of mixed BCs were designed in the numerical simulation as described in Table 1 in which x_2 direction is the loading direction. For boundary condition 1 (BC1), uniform displacements are imposed on the faces perpendicular to the loading direction without friction. Other faces parallel to the loading direction are traction free. This boundary condition is used to simulate the experimental setup in the mechanical test. For boundary condition 2 (BC2), the same conditions are set for the faces perpendicular to the loading direction; however the faces parallel to the loading direction remain straight and parallel during deformation to simulate an interior domain compatible with the surrounding material. Therefore, BC2 is periodic mechanically, but not microstructurally since the pores on opposing edges are not continuous. The boundaries for 2D models are the same as those applied

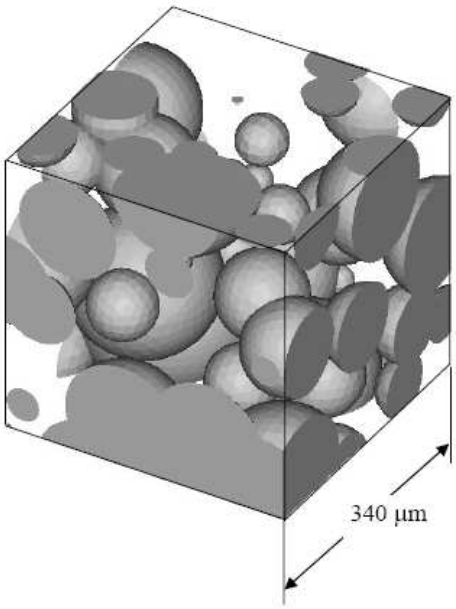

Figure 5. Geometry of the 3D model with porosity of 48% in a 340 μm cube.

to the left, right, top, and bottom faces of the 3D models to impose uniaxial compressive loading. Note that 2D models are restricted to uniaxial and biaxial load cases.

3. Results and discussion

3.1. ***Macroscopic response.*** The uniaxial stress-strain responses predicted by the sixteen individual 2D simulations (eight models deformed along x_1 and x_2 directions) of the 2D-1000, 2D-2000, 2D-3000, and 2D-4000 models under the two mixed BCs are shown in Figure 6. These collected results reveal that as 2D window size increases from 1000 μm to 4000 μm, the dispersion of the predicted stress-strain curves for each BC decreases. The range of the two groups of stress-strain curves associated with BC1 and BC2 also become smaller. The average responses of the sixteen individual 2D simulations under the two BCs

Model Face	Boundary Condition 1	Boundary Condition 2
Top ($x_2 = a$)	$u_2 = -0.01a; \quad t_1 = t_3 = 0$	$u_2 = -0.01a; \quad t_1 = t_3 = 0$
Bottom ($x_2 = 0$)	$u_2 = 0; \quad t_1 = t_3 = 0$	$u_2 = 0; \quad t_1 = t_3 = 0$
Left ($x_1 = 0$)	$t_1 = t_2 = t_3 = 0$	$u_1 = -\bar{u}_1; \quad t_2 = t_3 = 0$
Right ($x_1 = a$)	$t_1 = t_2 = t_3 = 0$	$u_1 = \bar{u}_1; \quad t_2 = t_3 = 0$
Front ($x_3 = a$)	$t_1 = t_2 = t_3 = 0$	$u_3 = \bar{u}_3; \quad t_1 = t_2 = 0$
Back ($x_3 = 0$)	$t_1 = t_2 = t_3 = 0$	$u_3 = -\bar{u}_3; \quad t_1 = t_2 = 0$

Table 1. Boundary conditions ($\bar{u}_1$ and $\bar{u}_3$ are displacements of the four side faces upon loading on the top).

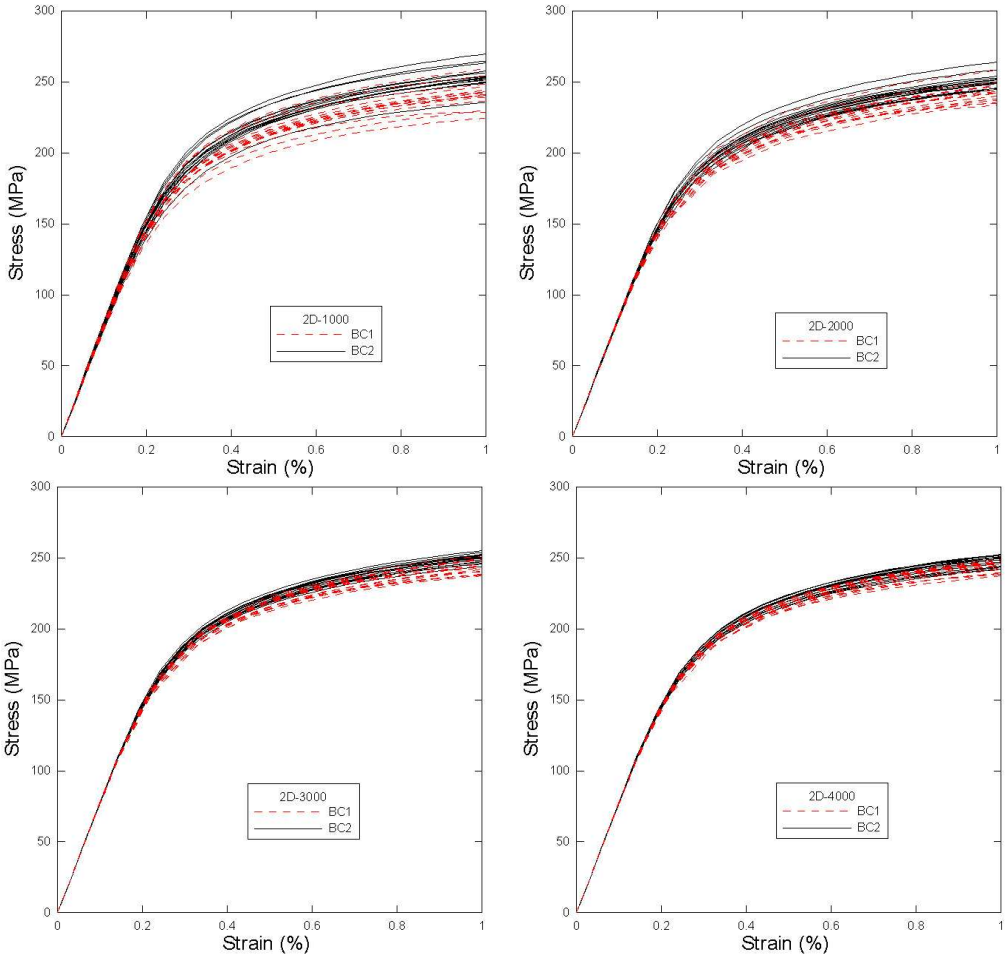

Figure 6. Macroscopic stress-strain responses predicted by the sixteen individual simulations of 2D-1000 (top left), 2D-2000 (top right), 2D-3000 (bottom left), and 2D-4000 models (bottom right) associated with the two mixed boundary conditions.

converge to a common value as the window size increases as shown in Figure 7. The convergence trend of the two BCs suggests BC1 is slightly underrestrictive which is similar to UTBC, and BC2 is slightly overrestrictive, which is similar to UDBC. The asymptotic relationship of the average elastic modulus and overall stress at 1% strain corresponding to the length scale of the window is illustrated in Figure 8. The overall averages of all thirty-two responses (eight models deformed along x_1 and x_2 directions under BC1 and BC2) for each model group are shown in Figure 9, and the curves are nearly indistinguishable.

The observations presented in the figures are confirmed in Table 2, which shows the 2D model predictions for elastic modulus and overall stress at 1% uniaxial strain. We see here that under BC1 and BC2 the standard deviation of elastic modulus decreases from 2.34% and 2.12% for the 2D-1000 models to 0.45% and 0.44% for the 2D-4000 models. The overall stress decreases from 3.69% and 3.0% to 1.55% and 1.44%, respectively. For all thirty-two responses for the two BCs, the standard deviation decreases

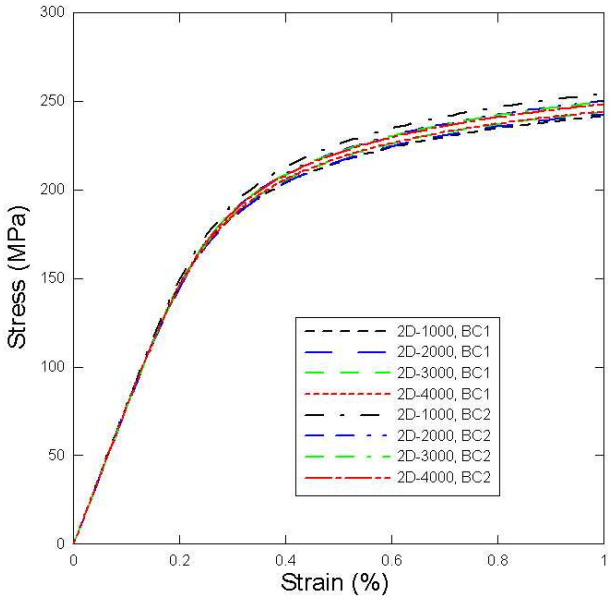

Figure 7. Macroscopic stress-strain responses averaged over the sixteen individual simulations of 2D-1000, 2D-2000, 2D-3000, and 2D-4000 models associated with the two mixed boundary conditions.

		E (GPa)		σ (MPa)	
		AVG.	SD%	AVG.	SD%
2D-1000	BC1	78.06	2.34	241.37	3.69
	BC2	79.08	2.12	254.30	3.00
	BC1.2avg	***78.57***	***2.29***	***247.84***	***4.23***
2D-2000	BC1	77.19	0.97	242.59	2.61
	BC2	77.92	0.91	250.1	2.10
	BC1.2avg	***77.56***	***1.04***	***246.27***	***2.79***
2D-3000	BC1	77.67	0.54	243.72	1.92
	BC2	78.03	0.51	249.45	1.29
	BC1.2avg	***77.85***	***0.57***	***246.59***	***1.99***
2D-4000	BC1	77.69	0.45	244.04	1.55
	BC2	78	0.44	248.15	1.44
	BC1.2avg	***77.85***	***0.48***	***246.09***	***1.7***

Table 2. 2D model predictions for elastic modulus and overall stress in loading direction at 1% uniaxial strain.

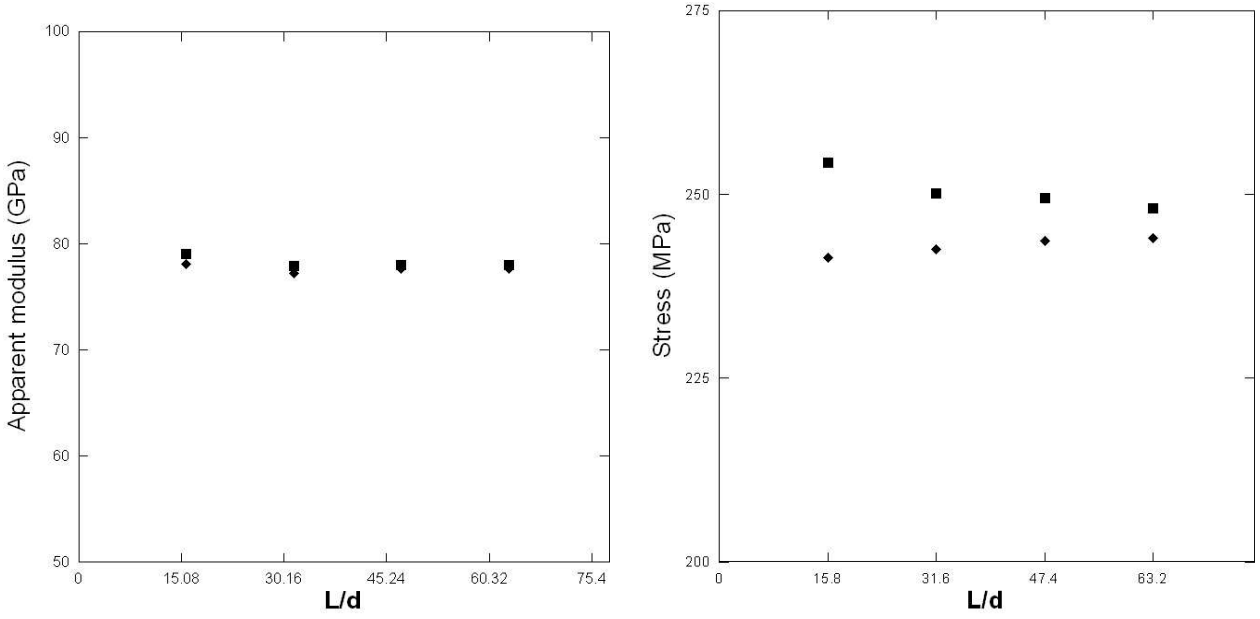

Figure 8. Apparent modulus (left) and overall average stress (right) at 1% far-field strain associated with the two mixed boundary conditions as a function of the ratio of the window size to pore diameter.

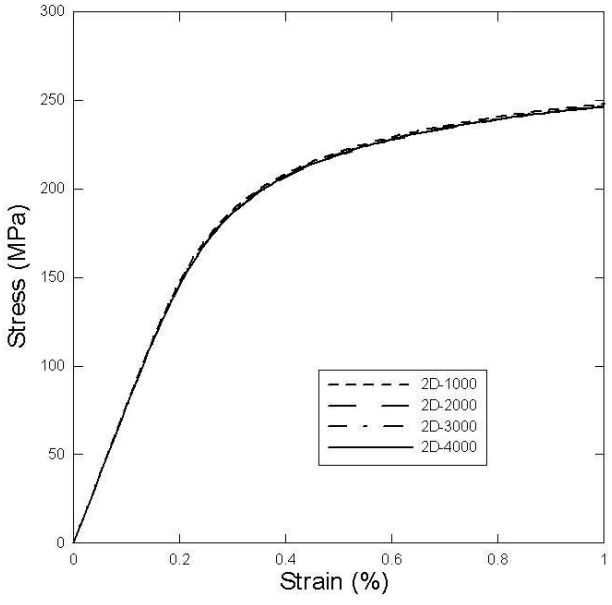

Figure 9. Macroscopic stress-strain responses averaged over the thirty-two individual simulations of 2D-1000, 2D-2000, 2D-3000, and 2D-4000 models.

from 2.29% to 0.48% for elastic modulus and 4.23% to 1.7% for overall stress. As the scatter of the data decreases, the overall averages (BC1_2avgs) of each model group under the two BCs remain almost constant. For example, only 0.71% difference exists between the averages of the overall stresses of the 2D-1000 and 2D-4000 models.

Based on the observations above, we believe that the averages over the individual simulations under the two BCs should be close to an "exact" solution. We derive this hypothesis from the homogenization convergence assumption: estimates under different BCs converge to the effective response as the calculated domain approaches Hill's RVE for locally heterogeneous but globally homogeneous microstructures [Hazanov and Huet 1994; Hollister and Kikuchi 1992; Huet 1990; Jiang et al. 2001a; Ostoja-Starzewski 1998; Pecullan et al. 1999; Sab 1992; Terada et al. 2000]. Therefore, we conclude that a number of small models can obtain convergent results equivalent to larger models. At the same time, since the averaged stress-strain curves associated with BC1 and BC2 approach the "exact" solution which lies in between, the error of the predicted result of each BC to the effective one can be estimated. For example, since 1.7% difference exists between the average stresses at 1% strain for the 2D-4000 models under the two BCs as shown in Figure 8, the error of the result from each BC to the "exact" solution should be less than 1.7%, and the error of the average of BC1 and BC2 (BC1_2avg in Table 2) less than 0.85%. This method suggests that by selecting a certain number of models associated with two selected slightly underrestrictive and overrestrictive boundary conditions providing opposite bias of the result, both the convergent result and the degree of accuracy can be estimated.

The fast homogenization achieved here occurs because all the models selected are of fixed porosity and are subjected to the two mixed BCs. These conditions are different from the findings in [Kanit et al. 2003]. In their work on the determination of the RVE size, small models have large variance of volume fractions, a fact which leads to large variance in results. They also showed that bias exists for the average of predictions of a number of small domains associated with one periodic BC, and that the bias decreases to zero as the size of analyzed domains reaches a certain level. With this one-sided approach, variance can be eliminated only by increasing domain size.

The study can also be generalized to 3D FE analysis. The uniaxial stress-strain responses predicted by the twelve individual 3D simulations (four models deformed along the three perpendicular directions) of the 3D-170 and 3D-340 models under the two mixed BCs are shown in Figure 10. Similar to the 2D simulations, the scatter of the curves decreases as the size of the 3D models increases. The average stress-strain curves over the individual simulations associated with BC1 and BC2 for 3D-340 models are closer than 3D-170 models as shown in Figure 11. The overall averages of the stress-strain responses for each model group of both the BCs (BC1_2avg) are plotted in Figure 12 and the two curves almost superpose. The results for elastic modulus and overall average stress at 1% uniaxial strain for the 3D models are shown in Table 3. For all twenty-four responses for the two BCs, the standard deviation for modulus decreases from 3.05% for 3D-170 models to 0.97% for 3D-340 models, and from 5.95% to 2.47% for overall average stress. The two mixed BCs offer biased predictions as in the 2D models. Therefore, the discussion and conclusions based on the 2D FE analyses above hold true for the 3D FE study. We presented a detailed comparison between 2D and 3D FE simulations in [Shen and Brinson 2007], and found that the macroscopic responses predicted by the 3D models are in reasonable agreement with the experimental and theoretical results. The macroscopic plastic responses predicted by 2D models are lower than those predicted by 3D models, while the elastic responses are close. 2D models overpredict

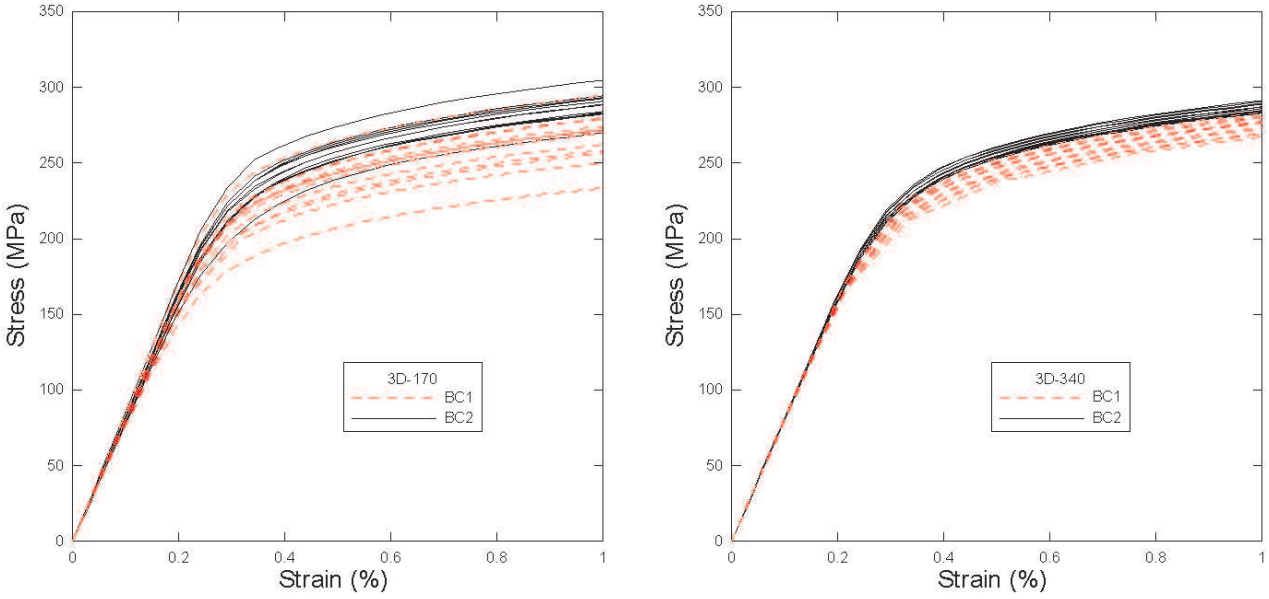

Figure 10. Macroscopic stress-strain responses predicted by the twelve individual simulations of 3D-170 (left) and 3D-340 (right) models associated with the two mixed boundary conditions.

the probability of high Von Mises stress and equivalent plastic strain and therefore overestimate the failure probability for porous materials.

It should be noted that the current BCs for the model groups are only appropriate for the simulation of titanium foam at low porosities (less than 25%) under uniaxial loading conditions. However, this study elucidates a method to find relatively small RVEs for heterogeneous materials, especially for the difficult case of high contrast properties between the phases. As the material is foamed to high porosity, pores are connected to form larger pores complicating the microstructure as shown in Figure 5. The uniaxial stress-strain responses predicted by the 3D model with higher porosity of 48% (the 3D model deformed

		E (GPa)		σ (MPa)	
		AVG.	SD%	AVG.	SD%
3D-170	BC1	80.36	3.26	266.73	5.93
	BC2	81.93	2.62	287.91	2.97
	BC1.2avg	***81.15***	***3.05***	***277.32***	***5.95***
3D-340	BC1	80.61	0.91	275.63	1.89
	BC2	81.42	0.78	286.66	0.96
	BC1.2avg	***81.01***	***0.97***	***281.14***	***2.47***

Table 3. 3D model predictions for elastic modulus and overall stress in loading direction at 1% uniaxial strain.

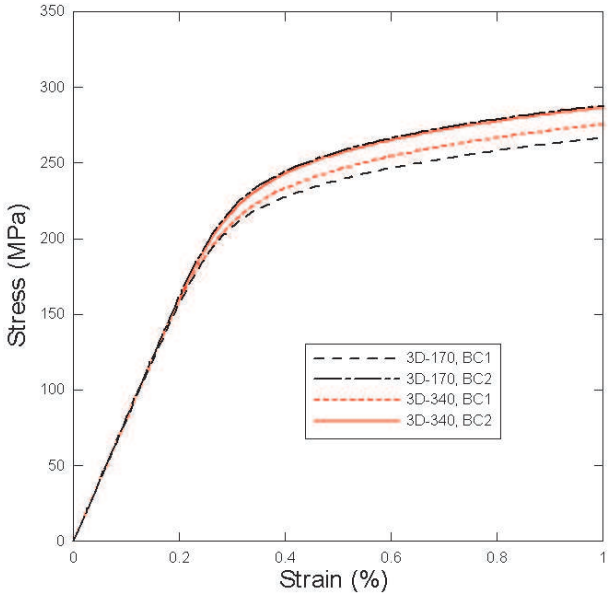

Figure 11. Macroscopic stress-strain responses averaged over the twelve individual simulations of 3D-170 and 3D-340 models associated with the two mixed boundary conditions.

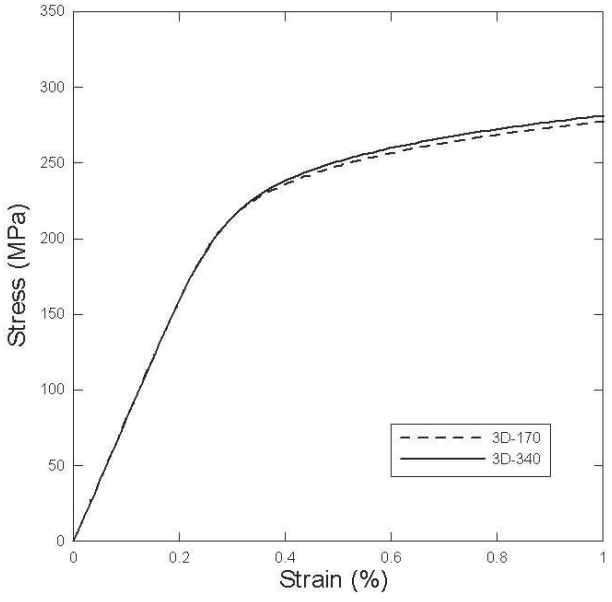

Figure 12. Macroscopic stress-strain responses averaged over the twenty-four individual simulations of 3D-170 and 3D-340 models.

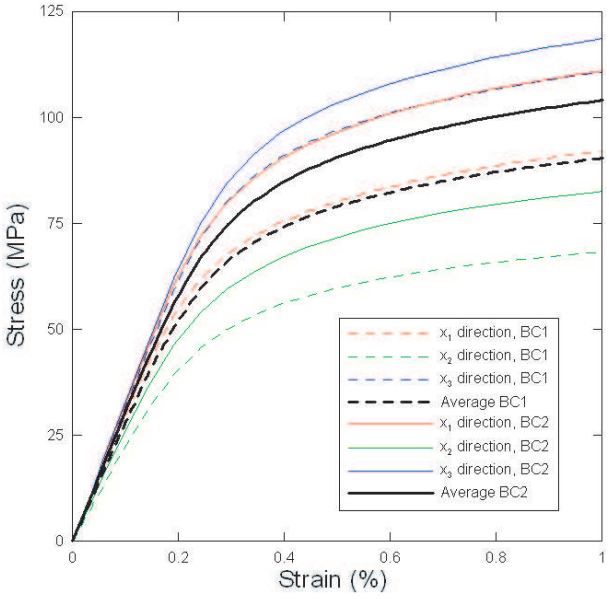

Figure 13. Macroscopic stress-strain responses predicted by the 3D model of 48% porosity associated with the two mixed boundary conditions.

along x_1, x_2 and x_3 directions) under the two mixed BCs are shown in Figure 13. The results indicate a much larger scatter than the 3D-340 models which have the same model size but lower porosity. The convergent response prediction for titanium foam at high porosity is therefore quite challenging and will be the focus of our future work. We can expect that more analyzed domains are needed to obtain a convergent result while using the boundary conditions which provide biased error.

3.2. ***Microscopic response.*** Microscopic field variable distributions are very important for failure analysis because failure is a local event rather than a volume averaged event. The Von Mises stress distributions in the matrices of all the 2D models deformed along x_1 and x_2 directions under 1% macroscopic strain are plotted in Figure 14. Since BC1 is less restrictive than BC2, the distributions of Von Mises stress under BC1 are broader than those under BC2. As with macroscopic responses, as model size increases, the curves become less dispersed. Both the mean value and standard deviation of the Von Mises stress distribution converge with increasing model size. For example, the maximum difference of the mean values of Von Mises stress under BC2 is 8.5% for 2D-1000 models and 4.2% for 2D-4000 models. The average distribution curves of the sixteen individual simulations of 2D-1000, 2D-2000, 2D-3000, and 2D-4000 models associated with the two mixed BCs converge to a common mean value and a common standard deviation as shown in Figure 15. The difference between the averaged mean values under BC1 and BC2 for 2D-1000 models is 5.9% and for 2D-4000 models is 1.8%. This common mean value and common standard deviation of the Von Mises stress distribution is clearly seen in Figure 16, in which the overall averages of the total thirty-two distribution curves for all the 2D models are plotted. Although not shown here, the equivalent plastic strain distribution follows a similar convergence trend.

To see the influence of the BCs on the microscopic distributions for models with different sizes, the equivalent plastic strain distributions predicted by one of the 2D-1000 and 2D-4000 models under 1% far

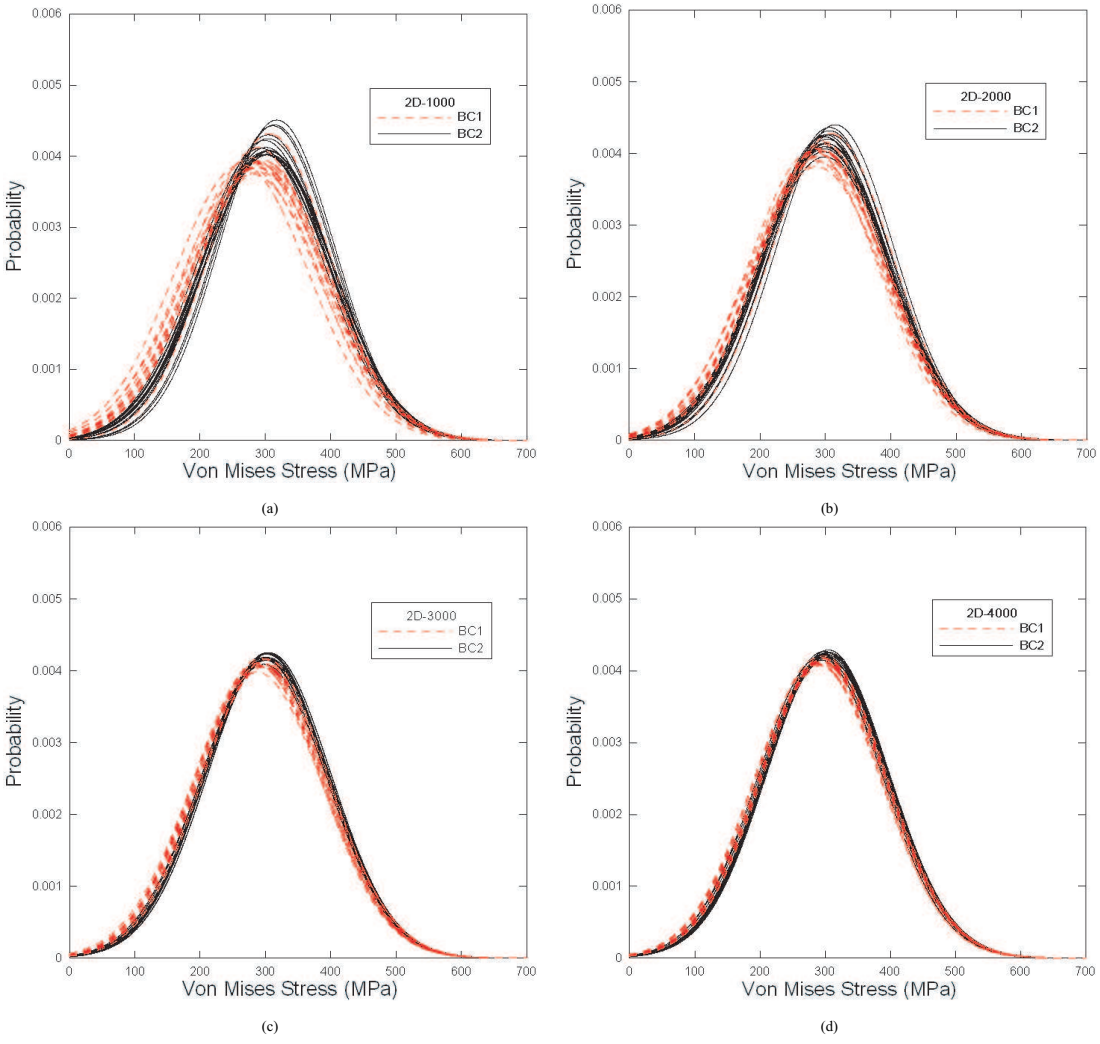

Figure 14. Von Mises stress distributions predicted by the sixteen individual simulations of (a) 2D-1000, (b) 2D-2000, (c) 2D-3000, and (d) 2D-4000 models associated with the two mixed boundary conditions.

field strain were plotted in Figure 17. In the 2D-1000 model, plastic strain distributions are influenced by BCs such that differences exist even in the middle of the analyzed domain. In the 2D-4000 models, differences in the plastic strain distributions away from the boundaries become negligible. However, the deficiency of the individual small 2D models can be compensated by averaging results of more models associated with the two BCs.

The accumulated frequencies of the Von Mises stress of the 2D models are plotted in Figure 18. These values were obtained by calculating the percentage of all the matrix elements exceeding a certain value in each model group. As is evident in Figure 18, the results of the Von Mises stress distribution of the 2D models under BC1 and BC2 also converge in the same manner as the macroscopic stress-strain responses.

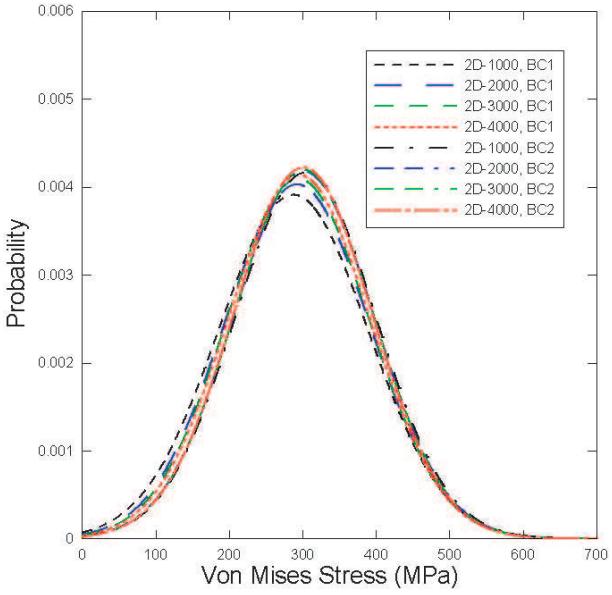

Figure 15. Von Mises stress distributions averaged over the sixteen individual simulations of 2D-1000, 2D-2000, 2D-3000, and 2D-4000 models associated with the two mixed boundary conditions.

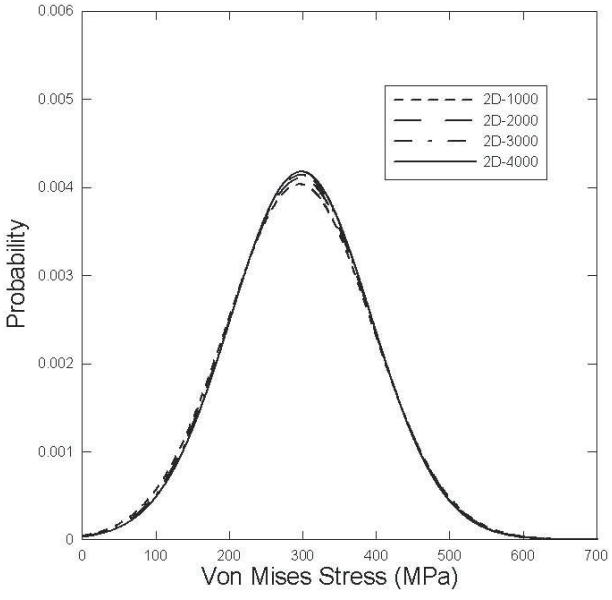

Figure 16. Von Mises stress distributions averaged over the thirty-two individual simulations of 2D-1000, 2D-2000, 2D-3000, and 2D-4000 models.

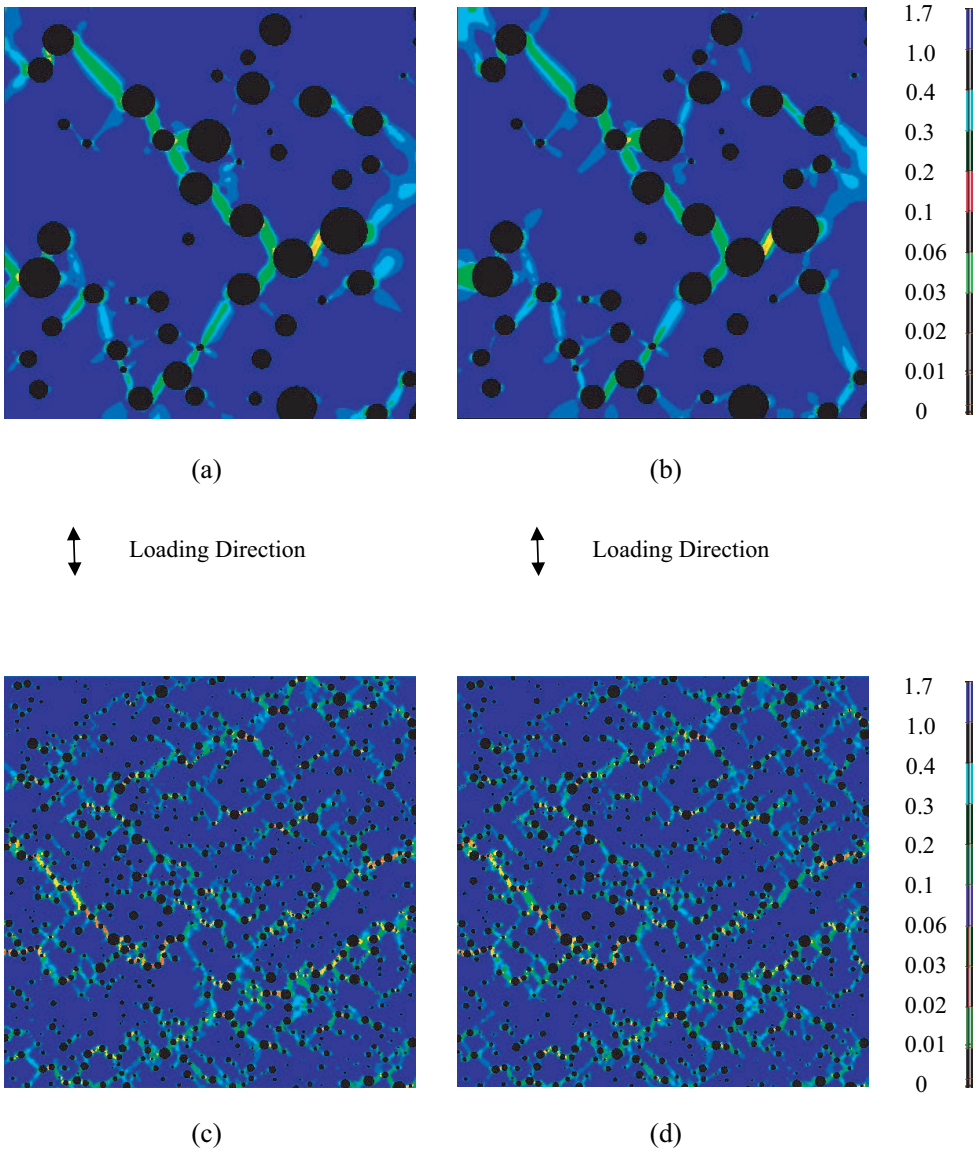

Figure 17. Equivalent plastic strain distribution predicted by (a) one of 2D-1000 model under BC1, (b) the 2D-1000 model under BC2, (c) one of 2D-4000 model under BC1, and (d) the 2D-4000 model under BC2.

With this frequency averaged over all the 2D simulations under the two BCs, a relatively accurate result can be obtained by the 2D-1000 model, one which is very close to the prediction of 2D-4000 models as shown in Figure 19. Therefore the convergence discussion on the macroscopic responses should be still valid for the microscopic variable statistic distributions.

To generalize the microscopic study to 3D FE analysis, the corresponding results of Von Mises stress predicted by the twelve individual 3D simulations (four models deformed along the three perpendicular

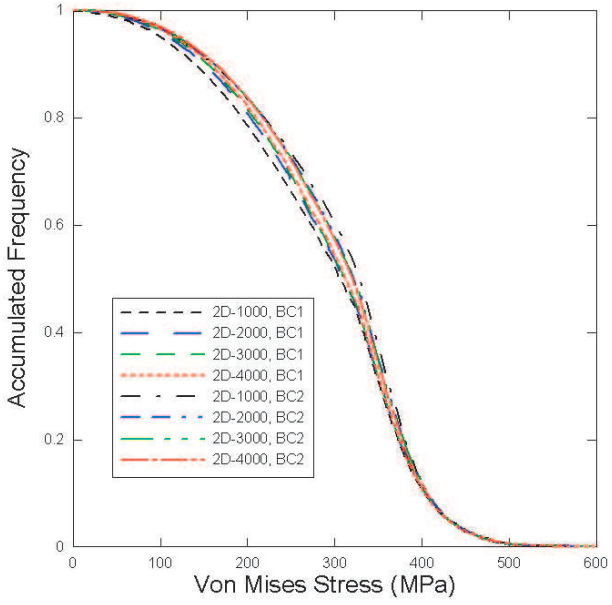

Figure 18. Accumulative frequency of Von Mises stress exceeding a certain value predicted by 2D-1000, 2D-2000, 2D-3000, and 2D-4000 models associated with the two mixed boundary conditions.

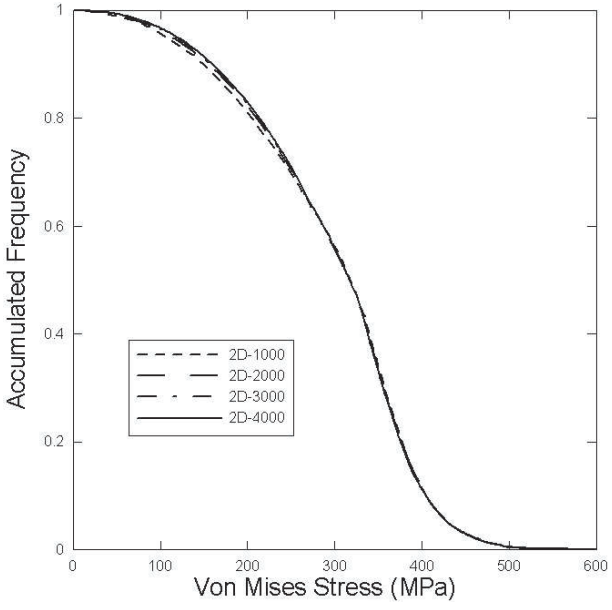

Figure 19. Accumulative frequency of Von Mises stress exceeding a certain value, averaged over the two mixed boundary conditions predicted by 2D-1000, 2D-2000, 2D-3000, and 2D-4000 models.

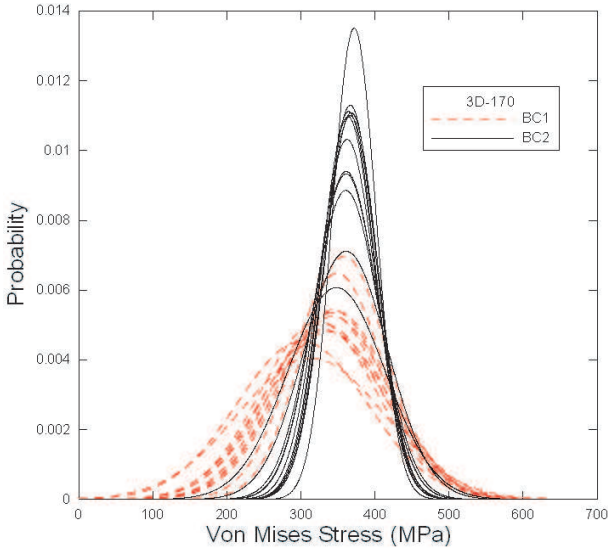

(a)

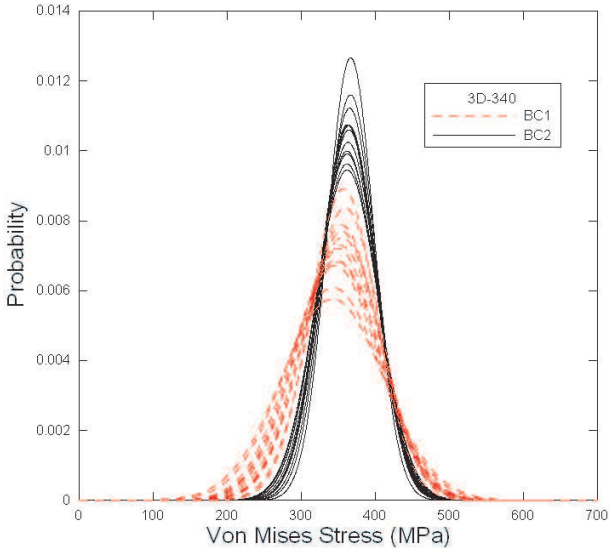

(b)

Figure 20. Von Mises stress distribution predicted by the twelve individual simulations of (a) 3D-170 and (b) 3D-340 models associated with the two mixed boundary conditions.

directions) of the 3D-170 and 3D-340 models under the two mixed BCs are shown in Figure 20. Similar convergence trend can be observed as the size of the 3D models increases. The average responses over the individual simulations associated with the two BCs are shown in Figure 21. The difference between the mean Von Mises stress at 1% strain under BC 1 and BC 2 for the 3D-170 models is 8.5% and for

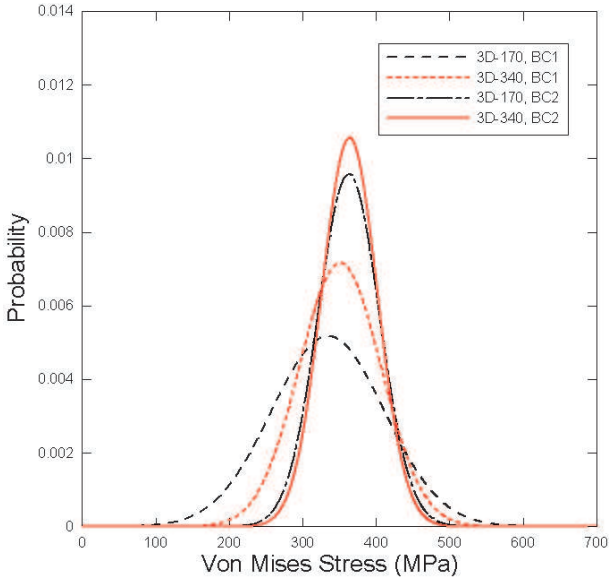

Figure 21. Von Mises stress distributions averaged over the twelve individual simulations of 3D-170 and 3D-340 models associated with the two mixed boundary conditions.

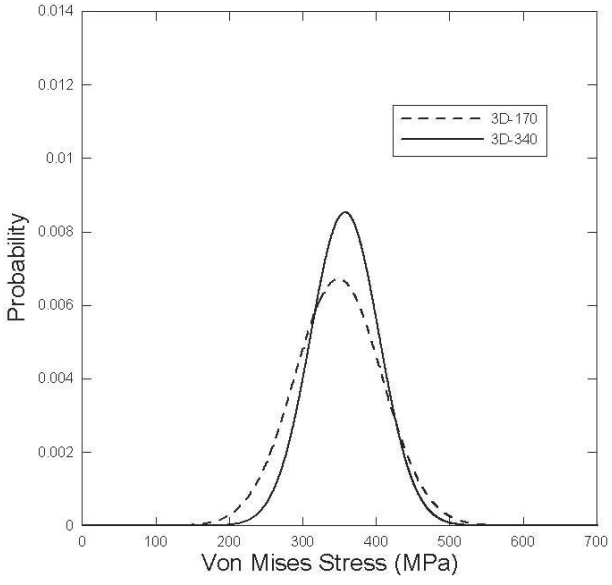

Figure 22. Von Mises stress distributions averaged over the twenty-four individual simulations of 3D-170 and 3D-340 models.

3D-340 models is 3.6%. The overall averages of the total responses for each 3D model group are shown in Figure 22. Although the curves are not as close as 2D models, the convergence trend is similar to the 2D study. The accumulated frequencies of the Von Mises stress of the 3D models are plotted in Figure

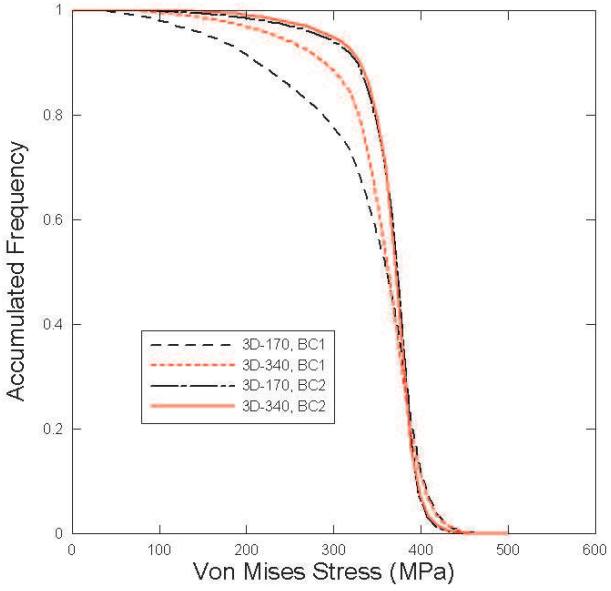

Figure 23. Accumulative frequency of Von Mises stress exceeding a certain value predicted by 3D-170 and 3D-340 models associated with the two mixed boundary conditions.

23. The frequency averaged over all the 3D simulations under the two BCs is shown in Figure 24. A similar convergence trend can also been observed. We expect that as the 3D models increase to 640 μm, the individual stress and strain curves would become more convergent. However, due to computational limitations, it is not practical to analyze the model with a 640 μm side length. Since the two BCs are bounds for the properties, the "exact" effective response should lie in between. In other words, since the difference between the mean Von Mises stress at 1% strain for the 3D-340 models under BC1 and BC2 is 3.6%, the average should be within 1.8% of the exact solution.

We find that for microscopic response, the 3D models predict higher mean Von Mises stress than 2D models, but relatively uniform distributions with smaller standard deviation. For example, the distribution of the Von Mises stress is 357.7 ± 46.7 MPa for 3D-340 models and 298 ± 95.5 MPa for 2D-4000 models. Our companion work [Shen and Brinson 2007] gives an extensive comparison between the stress and strain distribution.

4. Conclusions

In this study, we present an approach to determine RVEs of porous titanium. The method adopts the RVE concept of [Kanit et al. 2003] according to which the RVEs can be small domains as long as the average of the small domains provides an unbiased result. Since the estimates associated with uniform traction and displacement BCs provide the lower and higher bounds for the effective properties providing the largest bias, two mixed boundary conditions are therefore designed to obtain results with a smaller bias. Four groups of 2D models and two groups of 3D models with various sizes and fixed porosity were constructed based on a simulated microstructure of an experimental material. As the length scale

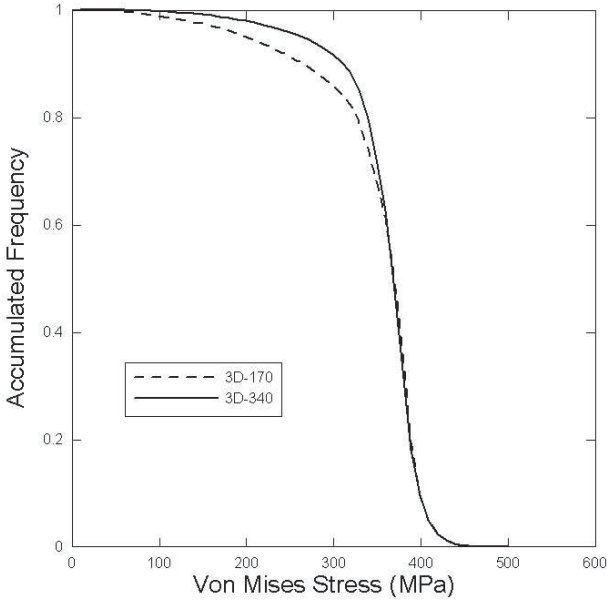

Figure 24. Accumulative frequency of Von Mises stress exceeding a certain value, averaged over the two mixed boundary conditions predicted by 3D-170 and 3D-340 models.

of the model increases, the individual responses of models become less dispersed. At the same time, the averages of the estimates associated with the two mixed BCs show opposite bias and converge to a common value. The error can be estimated and a convergent result can be obtained from relatively small models by averaging the responses associated with the two mixed BCs. The method developed here can be used to simulate microstructures of real materials. Although we have studied only a special case for titanium foam at low porosity under uniaxial loading, this method elucidates an approach for studying other heterogeneous materials, including those with a higher volume fraction of pores to inclusions. By choosing appropriate boundary conditions, a convergent result can be achieved by averaging the results of a number of small analyzed domains. The number of the domains needed will depend on the nature of the microstructure, the designed boundary, and the domain size.

References

[ABAQUS 2004] *ABAQUS standard user's manual*, version 6.4, Hibbitt Karlsson Sorensen Inc., Pawtucket, RI, 2004.

[ASM 2002] *Atlas of stress-strain curves*, 2nd ed., ASM International, Materials Park, OH, 2002.

[Banhart 2001] J. Banhart, "Manufacture, characterisation and application of cellular metals and metal foams", *Prog. Mater. Sci.* **46**:6 (2001), 559–632.

[Bouyge et al. 2002] F. Bouyge, I. Jasiuk, S. Boccara, and M. Ostoja-Starzewski, "A micromechanically based couple-stress model of an elastic orthotropic two-phase composite", *Eur. J. Mech. A: Solids* **21**:3 (2002), 465–481.

[Chang et al. 1996] Y. S. Chang, M. Oka, M. Kobayashi, H. O. Gu, Z. L. Li, T. Nakamura, and Y. Ikada, "Significance of interstitial bone ingrowth under load-bearing conditions: a comparison between solid and porous implant materials", *Biomaterials* **17**:11 (1996), 1141–1148.

[Davis et al. 2001] N. G. Davis, J. Teisen, C. Schuh, and D. C. Dunand, "Solid-state foaming of titanium by superplastic expansion of argon-filled pores", *J. Mater. Res.* **16**:5 (2001), 1508–1519.

[Drugan and Willis 1996] W. J. Drugan and J. R. Willis, "A micromechanics-based nonlocal constitutive equation and estimates of representative volume element size for elastic composites", *J. Mech. Phys. Solids* **44**:4 (1996), 497–524.

[Dunand 2004] D. C. Dunand, "Processing of titanium foams", *Adv. Eng. Mater.* **6**:6 (2004), 369–376.

[Gibson and Ashby 1997] L. Gibson and M. Ashby, *Cellular solids: Structure and properties*, 2nd ed., Cambridge University Press, New York, 1997.

[Gusev 1997] A. A. Gusev, "Representative volume element size for elastic composites: A numerical study", *J. Mech. Phys. Solids* **45**:9 (1997), 1449–1459.

[Hazanov 1999] S. Hazanov, "On apparent properties of nonlinear heterogenerous bodies smaller than the representative volume", *Acta Mech.* **134**:3–4 (1999), 123–134.

[Hazanov and Huet 1994] S. Hazanov and C. Huet, "Order relationships for boundary conditions effect in heterogeneous bodies smaller than the representative volume", *J. Mech. Phys. Solids* **42**:12 (1994), 1995–2011.

[Hill 1963] R. Hill, "Elastic properties of reinforced solids: Some theoretical principles", *J. Mech. Phys. Solids* **11**:5 (1963), 357–372.

[Hollister and Kikuchi 1992] S. J. Hollister and N. Kikuchi, "A comparison of homogenization and standard mechanics analyses for periodic porous composites", *Comput. Mech.* **10**:2 (1992), 73–95.

[Huet 1990] C. Huet, "Application of variational concepts to size effects in elastic heterogeneous bodies", *J. Mech. Phys. Solids* **38**:6 (1990), 813–841.

[Jiang et al. 2001a] M. Jiang, K. Alzebdeh, I. Jasiuk, and M. Ostoja-Starzewski, "Scale and boundary conditions effects in elastic properties of random composites", *Acta Mech.* **148** (2001), 63–78.

[Jiang et al. 2001b] M. Jiang, M. Ostoja-Starzewski, and I. Jasiuk, "Scale-dependent bounds on effective elastoplastic response of random composites", *J. Mech. Phys. Solids* **49**:3 (2001), 655–673.

[Kanit et al. 2003] T. Kanit, S. Forest, I. Galliet, V. Mounoury, and D. Jeulin, "Determination of the size of the representative volume element for random composites: statistical and numerical approach", *Int. J. Solids Struct.* **40**:13–14 (2003), 3647–3679.

[Li et al. 1998] M. Li, S. Ghosh, T. N. Rouns, H. Weiland, O. Richmond, and W. Hunt, "Serial sectioning method in the construction of 3-D microstructures for particle-reinforced MMCs", *Mater. Charact.* **41**:2–3 (1998), 81–95.

[Li et al. 2004] H. Li, S. M. Oppenheimer, S. I. Stupp, D. C. Dunand, and L. C. Brinson, "Effects of pore morphology and bone ingrowth on mechanical properties of microporous titanium as an orthopaedic implant material", *Mater. Trans.* **45**:4 (2004), 1124–1131.

[Murray and Dunand 2003] N. G. D. Murray and D. C. Dunand, "Microstructure evolution during solid-state foaming of titanium", *Compos. Sci. Technol.* **63**:16 (2003), 2311–2316.

[Ostoja-Starzewski 1998] M. Ostoja-Starzewski, "Random field models of heterogeneous materials", *Int. J. Solids Struct.* **35**:19 (1998), 2429–2455.

[Pecullan et al. 1999] S. Pecullan, L. V. Gibiansky, and S. Torquato, "Scale effects on the elastic behavior of periodic and hierarchical two-dimensional composites", *J. Mech. Phys. Solids* **47**:7 (1999), 1509–1542.

[Sab 1992] K. Sab, "On the homogenization and the simulation of random materials", *Eur. J. Mech. A: Solids* **11**:5 (1992), 585–607.

[Shen and Brinson 2007] H. Shen and L. C. Brinson, "Finite element modeling of titanium foam", *Int. J. Solids Struct.* **44**:1 (2007), 320–335.

[Shen et al. 2006] H. Shen, S. M. Oppenheimer, D. C. Dunand, and L. C. Brinson, "Numerical modeling of pore size and distribution in foamed titanium", *Mech. Mater.* **38**:8–10 (2006), 933–944.

[Spoerke et al. 2005] E. D. Spoerke, N. G. Murray, H. Li, L. C. Brinson, D. C. Dunand, and S. I. Stupp, "A bioactive titanium foam scaffold for bone repair", *Acta Biomater.* **1**:5 (2005), 523–533.

[Terada et al. 2000] K. Terada, M. Horib, T. Kyoyac, and N. Kikuchi, "Simulation of the multi-scale convergence in computational homogenization approaches", *Int. J. Solids Struct.* **37**:16 (2000), 2285–2311.

[Tobias and Trindade 1995] P. A. Tobias and D. C. Trindade, *Applied reliability*, Van Nostrand Reinhold, New York, 1995.

[Wen et al. 2002a] C. E. Wen, Y. Yamada, K. Shimojima, Y. Chino, T. Asahina, and M. Mabuchi, "Processing and mechanical properties of autogenous titanium implant materials", *J. Mater. Sci.: Mater. Med.* **13**:4 (2002), 397–401.

[Wen et al. 2002b] C. E. Wen, Y. Yamada, K. Shimojima, Y. Chino, T. Hosokawa, and M. Mabuchi, "Novel titanium foam for bone tissue engineering", *J. Mater. Res.* **17**:10 (2002), 2633–2639.

Received 11 Jan 2006. Accepted 12 May 2006.

HUI SHEN: h-shen@onu.edu
Mechanical Engineering Department, Ohio Northern University, Ada, OH 45810, United States
http://www2.onu.edu/%7Ehshen/

L. CATHERINE BRINSON: cbrinson@northwestern.edu
Mechanical Engineering Department, Northwestern University, Technological Institute B224, 2145 Sheridan Road, Evanston, IL 60208, United States
http://www.mech.northwestern.edu/web/people/faculty/brinson.htm